

Corrosion Electrochemical Behavior of PCB-HASL Circuit Boards in NaHSO₃/Na₂SO₃ Solution: Postprint

Authors: Ding Kangkang, Xiao Kui, Zou Shiwen, DONG Chaofang, Zhao Ruitao, LI Xiaogang

Date: 2016-11-04T00:00:00+00:00

Abstract

The corrosion behavior and mechanism of hot air solder leveling lead-free tin-sprayed printed circuit boards (PCB-HASL) in simulated electrolytes of 0.1 mol/L NaHSO₃ and 0.1 mol/L NaHSO₃/Na₂SO₃ solutions with different pH values were investigated using electrochemical impedance spectroscopy (EIS) and scanning Kelvin probe (SKP) techniques. The effects of immersion time and pH value on the transformation of the corrosion mechanism were discussed, and the nucleation and propagation behaviors of corrosion products on the PCB-HASL surface were observed and analyzed by OM, SEM combined with EDS. The results indicate that in acidic NaHSO₃/Na₂SO₃ solution systems, the corrosion morphology of PCB-HASL specimens is similar to pitting corrosion, with corrosion pits accelerating and expanding during the early immersion stage, and the corrosion products are mainly Sn oxides and sulfates. NaHSO₃ solution can activate the surface of PCB-HASL specimens, and nucleation of corrosion pits occurs only during the initial immersion stage. In neutral or alkaline NaHSO₃/Na₂SO₃ solution systems, the formation of corrosion pits on the PCB-HASL specimen surface is suppressed, and the electrode reaction rate is limited by the transport process of the electrolyte solution through the oxide film to the electrode interface.

Full Text

Electrochemical Corrosion Behavior of PCB-HASL in NaHSO₃/Na₂SO₃ Solution

Kangkang Ding, Kui Xiao, Shiwen Zou, Chaofang Dong, Ruitao Zhao, Xiaogang Li

*Corrosion and Protection Center, University of Science and Technology Beijing,
Beijing 100083, China*

Abstract

With continuous innovation in electronic technology, printed circuit boards (PCBs) are developing toward further integration and miniaturization, while corrosion issues of PCBs have become increasingly prominent. Even trace amounts of corrosion products can seriously affect PCB reliability. To improve the corrosion resistance of PCBs, various surface finishing technologies have emerged, among which hot air solder leveling (HASL) technology has gained widespread application due to its low cost and excellent solderability.

In actual service environments, particularly when hygroscopic solid deposits are present or air reaches water saturation, a thin liquid film or droplets form on the PCB-HASL surface. Contaminant gases such as SO₂ dissolve in this film to create an electrolyte solution, initiating electrochemical corrosion beneath the electrolyte. Numerous studies have investigated the electrochemical corrosion behavior of various surface-finished PCBs—including copper-clad laminates (PCB-Cu), electroless nickel immersion gold (PCB-ENIG), and immersion silver (PCB-ImAg)—in different electrolytes. However, research on PCB-HASL material corrosion has primarily focused on tin whisker growth and fretting corrosion. Whiskering is an inherent characteristic of tin that particularly occurs on solder pads or tin-plated surfaces, causing PCB short-circuit failures. Compressive stress is generally considered a necessary condition for tin whisker growth, while high temperature and humidity are key factors accelerating this process. Other work has systematically studied effects of applied current, mechanical bending, and thermal annealing on tin whisker growth, finding that whiskers grew more densely on the compression side of bent tin-plated boards, while both thermal annealing and applied current reduced whisker density, though external current increased whisker length. Fretting corrosion represents another major corrosion form for tin-plated components, with research establishing fretting corrosion mechanisms and evaluation models showing that lubricants can significantly enhance the lifetime of tin-plated contacts.

Understanding the electrochemical corrosion mechanism of PCB-HASL materials in electrolyte solutions is urgently needed. This work investigates the corrosion behavior and mechanism of PCB-HASL materials in simulated electrolytes of 0.1 mol/L NaHSO₃ and 0.1 mol/L NaHSO₃/Na₂SO₃ solutions with different pH values, examining the influence of immersion time and pH on corrosion mechanism transitions to provide a data foundation and guidance for material selection and life assessment under actual service conditions.

Experimental Methods

PCB-HASL samples were used as experimental materials with the following basic parameters: FR-4 substrate 1.2 mm thick, Cu foil base 25 μm thick, and

spray tin layer thickness approximately 10 μm . The effective sample size was 10 mm \times 10 mm. Before experiments, samples were ultrasonically cleaned in acetone for 10 minutes, then in deionized water for 10 minutes, wiped with anhydrous ethanol, and air-dried for later use.

Analytical grade NaHSO₃ was used to prepare 0.1 mol/L NaHSO₃ solution (pH 4.5). Samples were immersed in this solution for various durations before electrochemical impedance spectroscopy (EIS) measurements. Experimental periods were 0.5, 1, 2, 3, 6, 12, 24, 36, 72, and 120 hours. Buffer solutions of NaHSO₃/Na₂SO₃ with different pH values (pH = 6, 7, 8, and pure Na₂SO₃ at pH 9.4) were prepared by mixing different ratios of 0.1 mol/L NaHSO₃ and Na₂SO₃, with pH monitored and controlled using a PHB-4 portable pH meter with an accuracy of ± 0.01 pH. EIS measurements in different pH buffer solutions were conducted uniformly after 2 hours of immersion. EIS measurements were performed using a PAR VMP3 multi-channel electrochemical workstation with a three-electrode system: PCB-HASL sample as working electrode, Pt sheet as auxiliary electrode, and saturated calomel electrode (SCE) as reference electrode. EIS tests scanned frequencies from 1×10^5 to 0.01 Hz with a perturbation potential of 10 mV. Data were fitted using ZSimpWin V3.20.

Surface corrosion morphology and corrosion product propagation were observed using a Keyence VHX-2000 optical microscope (OM) and FEI Quanta 250 environmental scanning electron microscope (SEM), combined with an Ametek Apollo-X X-ray energy dispersive spectrometer (EDS) for elemental composition analysis of corrosion products. The VHX-2000 microscope's built-in function was used to determine the coverage area of corroded regions using brightness mode with a threshold setting of 3 and area measurement precision of 0.1 μm^2 . Four random positions were measured for each sample period, with average values taken as final results.

Scanning Kelvin probe (SKP) tests were conducted on PCB-HASL samples after different immersion times using a PAR M370 scanning electrochemical workstation. The probe-to-sample distance was (100 ± 2) μm , vibration frequency 80 Hz, amplitude 30 μm , with step scan area mapping over a 2 mm \times 2 mm region. In-situ measurements were performed on the same location with position deviation of ± 100 μm . Laboratory environment was controlled at 25 $^\circ\text{C}$ temperature and relative humidity.

Results and Discussion

2.1.1 Surface Corrosion Morphology

[Figure 1: see original paper] shows the surface morphology of PCB-HASL samples immersed in 0.1 mol/L NaHSO₃ solution for different times. After 0.5 hours of immersion, numerous tiny corrosion pits appeared on the sample surface, indicating extremely poor corrosion resistance of PCB-HASL to NaHSO₃ solution. As immersion time progressed, the corroded area expanded rapidly and gradually coalesced. By 12 hours, nearly half the sample surface had corroded, with

white crystalline precipitates appearing in local regions. At 36 hours, the entire sample surface was almost completely corroded, with significantly increased white crystalline deposits. Corrosion further intensified by 120 hours.

The coverage ratio of corrosion products on PCB-HASL surface was calculated using the OM software, with experimental data fitted as shown in [Figure 2: see original paper]. Within the first 12 hours, the corrosion coverage ratio $R = 3.581t^{1.1}$ (where t is immersion time), indicating accelerated corrosion development. After 12 hours, $R = 30.76t^{-0.31}$, showing increased reaction resistance and decreased corrosion expansion rate.

2.1.2 Corrosion Products

[Figure 3: see original paper] shows the micro-morphology and EDS analysis results of PCB-HASL samples after different immersion times. After 0.5 hours, local damage to the spray tin layer formed numerous pits of varying sizes. With increasing immersion time, pits developed slowly in depth but expanded rapidly along the surface, with small pits gradually coalescing to create two distinct surface states: corroded regions with rough surfaces covered by granular corrosion products, and uncorroded regions maintaining relatively flat spray tin layers. EDS analysis showed that in corroded area A, the atomic ratio of O:Sn:Cu was 12.5:68.10:19.41, while in area B it was 20.76:1.35:38.15:39.74. The significantly increased oxygen content and detection of sulfur indicated that granular corrosion products were primarily tin oxides (SnO , SnO_2 , Sn(OH)_2 or Sn(OH)_4) and trace sulfate/sulfite compounds. After 36 hours, numerous long, clustered crystalline precipitates formed in corroded regions. EDS analysis of area C showed an atomic ratio of O:S:Sn:Cu = 42.26:10.46:40.88:6.20, suggesting the main components were SnSO_4 or SnOSO_4 .

2.1.3 Scanning Kelvin Probe Analysis

[Figure 4: see original paper] shows the Kelvin potential distribution on PCB-HASL sample surfaces after immersion in 0.1 mol/L NaHSO_3 solution for different times. According to SKP principles, measuring the electron work function of metal surfaces in air determines the surface Kelvin potential (E_{kp}), which has a linear relationship with the surface potential E_{corr} in air:

$$E_{kp} = E_{corr} + W_{ref} - E_{ref}/2$$

where W_{ref} is the electrode work function and $E_{ref}/2$ is the half-cell potential of the reference electrode (vibrating probe). Both terms are constants in a specific system, so E_{kp} variations reflect changes in surface potential state.

The surface Kelvin potential distribution in droplet regions was fitted using a Gaussian function, with fitting curves and parameters shown in [Figure 5: see original paper] and Table 1. The fitting formula is:

$$y = y_0 + (A/(\sqrt{2\pi})) \times \exp(-(x-x_0)^2/(2\sigma^2))$$

where A is a constant, y is the SKP potential distribution count, y is the vertical offset, x is the SKP potential value, μ is the expectation value (central position of potential distribution), and σ is the standard deviation of Gaussian distribution representing dispersion degree—larger σ indicates more dispersed potential distribution.

Before immersion, the PCB-HASL surface potential distribution was uniform, concentrated near -0.5558 V with small σ value. After 0.5 hours, NaHSO₃ activation decreased the surface potential to an expectation value of -0.6312 V, with localized regions showing further potential reduction. Darker regions in the potential map acted as anodes that corroded preferentially, becoming “pitting” sources, increasing overall potential distribution difference (σ increased from 0.0228 to 0.0276). Over time, small corrosion pits expanded rapidly. Corrosion product accumulation made electron escape difficult, raising potentials in corroded regions. The potential map showed these regions expanding gradually, with σ reaching maximum values and surface potential differences becoming extreme. At 36 hours, most surface areas had corroded with significantly increased potential, while local uncorroded regions remained at very low potential, consistent with surface morphology features. The overall potential expectation value rose to -0.4498 V. By 120 hours, increased corrosion product accumulation caused further potential elevation, with localized regions showing substantial potential increases due to crystalline product obstruction, reaching maximum potential differences.

2.1.4 Corrosion Electrochemical Behavior

EIS tests were conducted to investigate the electrochemical corrosion interface process and kinetic parameter evolution of PCB-HASL samples in 0.1 mol/L NaHSO₃ solution, with results shown in [Figure 6: see original paper]. After 0.5 hours, the Nyquist plot consisted of two capacitive arcs at medium-high frequency, an inductive arc at low frequency, and a straight line at approximately 45° to the x-axis at the lowest frequencies. The straight line indicates diffusion-controlled electrode reaction processes at low frequencies, demonstrating the hindering effect of surface oxide layers on interfacial ion diffusion. The inductive arc results from dynamic changes in oxide film thickness during pit nucleation. The equivalent circuit shown in [Figure 7a: see original paper] provided good fitting results, where R_s represents solution resistance, R_f and CPE_f represent resistance and capacitance of surface oxide/corrosion product films, CPE_{dl} represents double layer capacitance, R_{ct} represents charge transfer resistance, W represents Warburg diffusion impedance, R_L reflects resistance related to film generation/dissolution at pit nucleation sites, and L represents equivalent inductance related to film thickness changes at pit nucleation sites. At this stage, the sample surface was in the pit nucleation phase with increasing pit numbers.

When immersion time reached 1 hour, the corrosion mechanism remained unchanged though the low-frequency inductive arc contracted significantly, indi-

cating the pit initiation stage was nearing completion. By 2 hours, the inductive arc disappeared completely, marking the end of new pit formation and entry into rapid pit propagation stage. Until 6 hours, the Nyquist plot shape remained essentially unchanged, indicating consistent corrosion mechanisms. During this stage, the medium-frequency capacitive arc contracted severely. Since high-frequency arcs reflect surface film information while medium-low frequency arcs reflect electrode interface processes, this contraction indicates substantially decreased reaction resistance. The equivalent circuit in [Figure 7b: see original paper] was used for fitting, with results shown in Table 2. R_{ct} gradually decreased during the first 6 hours, indicating accelerated corrosion processes consistent with the trend shown in [Figure 2: see original paper]. At 12 hours, overall impedance increased due to significantly expanded corroded area.

When immersion time reached or exceeded 24 hours, the low-frequency diffusion impedance line disappeared. With most of the sample surface covered by corrosion products, the impedance spectrum primarily reflected reactions in corroded regions. Corrosion product accumulation partially isolated the electrolyte from the electrode interface, causing substantial R_{ct} increases and expanded low-frequency capacitive arcs. The equivalent circuit in [Figure 7c: see original paper] was used. Fitting data in Table 2 show that after 24 hours, film impedance increased with time and R_{ct} remained at high levels, indicating that accumulated corrosion products provided some protective effect on the substrate metal.

2.2 Effect of pH on Corrosion Behavior and Mechanism

2.2.1 Surface Corrosion Morphology Observation The effect of pH on PCB-HASL corrosion behavior was further investigated. Based on EIS results and morphology observations, the electrode system reached a relatively stable state between 2-6 hours, making this a suitable uniform immersion time. To minimize interference from corrosion products formed during immersion on subsequent EIS measurements, the final immersion time was set at 2 hours.

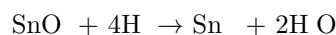
[Figure 8: see original paper] shows the surface morphology of PCB-HASL samples after 2 hours immersion in 0.1 mol/L $\text{NaHSO}_3/\text{Na}_2\text{SO}_3$ buffer solutions with different pH values. In 0.1 mol/L NaHSO_3 (pH = 4.5), numerous corrosion pits appeared. At pH = 6, pitting corrosion still occurred but with reduced number and size. As pH increased to neutral and alkaline conditions, pitting decreased significantly and corrosion approached general corrosion.

2.2.2 Corrosion Electrochemical Behavior EIS tests were conducted on samples after 2 hours immersion in buffer solutions of different pH values, with results shown in [Figure 9: see original paper]. At pH = 6, the EIS spectrum shape remained identical to that in 0.1 mol/L NaHSO_3 solution, indicating unchanged corrosion mechanisms at pH = 6, so the equivalent circuit in [Figure 7b: see original paper] was still used. However, at pH = 7, the EIS shape changed significantly, with Nyquist plots showing three capacitive arcs: high-frequency

arcs reflecting film information, medium-frequency arcs reflecting interface reactions (with diameters gradually increasing with pH), and low-frequency arcs resulting from finite-layer diffusion. The equivalent circuit in [Figure 10: see original paper] was used for fitting, where O and B reflect finite diffusion layer information. Fitting results in Table 3 show that R_{ct} increased substantially at neutral to alkaline pH, reducing solution aggressiveness. The dense surface oxide film created a finite diffusion layer with thickness equal to the oxide film, causing the low-frequency capacitive arc.

Discussion

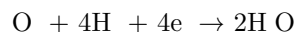
In typical atmospheric environments, tin plating surfaces possess a dense oxide film (SnO_2) that provides good substrate protection. However, when immersed in 0.1 mol/L NaHSO_3 simulated electrolyte, the PCB-HASL surface becomes activated and pit nucleation begins, with the surface oxide film undergoing dissolution:



Pit nucleation only occurs during the initial immersion stage. After exceeding 2 hours, new pit formation essentially ceases and the system enters rapid pit propagation stage. With expanding corroded areas, anodic dissolution occurs:



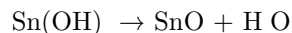
Since the NaHSO_3 solution is slightly acidic, it can accelerate or catalyze tin anodic dissolution. In fact, pure tin does not dissolve in acid solutions without oxidizing components due to its large hydrogen overpotential, but readily forms Sn^{2+} in oxygen-saturated acidic solutions. Therefore, the cathodic process under these experimental conditions should primarily be oxygen reduction:



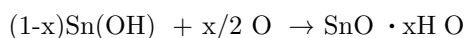
The overall reaction leads to:



$\text{Sn}(\text{OH})_2$ readily undergoes dehydration:



Additionally, O_2 may directly participate in electrode reactions or subsequent oxidation:



These reactions result in rough corroded surfaces with main corrosion products being SnO , SnO_2 , $\text{Sn}(\text{OH})_2$, or $\text{Sn}(\text{OH})_4$. With prolonged immersion, most of the sample surface becomes covered by corrosion products that provide some protective effect. Corrosion products continuously accumulate and tend toward a stable state, with generation and dissolution processes reaching dynamic equilibrium that maintains R_{ct} at relatively high levels.

Increasing solution pH reduces solution aggressiveness. At pH 6, the corrosion mechanism does not change significantly. However, at neutral to alkaline pH, pit formation is strongly suppressed and corrosion transitions to general corrosion. The relatively intact and dense oxide film layer limits electrolyte transport through the film to the electrode interface, creating a finite diffusion layer with thickness equal to the oxide film and causing substantial R_{ct} increases.

Conclusions

1. NaHSO₃ solution activates PCB-HASL sample surfaces. Initial corrosion occurs through local damage to the spray tin layer forming corrosion pits, which then expand primarily laterally along the surface.
2. During early immersion, samples experience accelerated corrosion with corrosion product coverage following $R = 3.581t^{1.1}$ (where t is immersion time). Corrosion products are mainly tin oxides and trace sulfates. During later stages, reaction resistance increases following $R = 30.76t^{0.31}$, with tin sulfate crystallization occurring and corrosion product films providing some substrate protection.
3. In neutral or alkaline NaHSO₃/Na₂SO₃ solution systems, pit formation on PCB-HASL samples is suppressed, and the electrode reaction rate is limited by electrolyte transport through the oxide film to the electrode interface.

References

- [1] Leygraf C, Graedel T. Atmospheric Corrosion. New York: John Wiley&Sons Inc, 2000: 142
- [2] Zhao Y, Lin C J, Li Y, Du R G, Wang J R. Acta Phys-Chim Sin, 2007; 23: 1342
- [3] Huang H L, Dong Z H, Chen Z Y, Guo X P. Corros Sci, 2011; 53: 1230
- [4] Zou S W, Li X G, Dong C F, Ding K K, Xiao K. Electrochim Acta, 2013; 114: 363.
- [5] Xiao K, Zou S W, Dong C F, Wu J S, Li X G. Sci Technol Rev, 2011; 29: 25
- [6] Qi H, Ganesan S, Pecht M. Microelectron Reliab, 2008; 48: 663
- [7] Shibutani T, Yu Q, Shiratori M, Pecht M G. Microelectron Reliab, 2008; 48: 1033
- [8] Fukuda Y, Osterman M, Pecht M. Microelectron Reliab, 2007; 47: 88
- [9] Park Y W, Sankara Narayanan T S N, Lee K Y. Tribol Int, 2008; 41: 616
- [10] Ammar I A, Darwish S, Khalil M W, Galal A. Materialwissenschaft und Werkstofftechnik, 1983; 14: 330
- [11] Jouen S, Hannoyer B, Piana O. Surf Interf Anal, 2002; 34: 192
- [12] Muller J. PhD Dissertation, Université Paris Est Marne-La-Vallée, 2010
- [13] Lundren G, Wernfors G, Yamaguchi T. Acta Crystallogr, 1982; 38B: 2357
- [14] Ahmed M A K, Fjellvag H, Kjekshus A. Acta Chem Scand, 1998; 52: 305
- [15] Zou S W, Li X G, Dong C F, Li H Y, Xiao K. Acta Metall Sin, 2012; 48:

687

- [16] Sun M, Xiao K, Dong C F, Li X G, Zhong P. Acta Metall Sin, 2011; 47:442
- [17] Li P H. Master Thesis, University of Science and Technology Beijing, 2011
- [18] Rohwerder M, Turcu F. Electrochim Acta, 2007; 53: 290
- [19] Cao C N, Zhan J Q. An Introduction to Electrochemical Impedance Spectroscopy. Beijing: Science Press, 2002: 54
- [20] Chen Z Y. PhD Dissertation, Huazhong University of Science & Technology, Wuhan, 2010
- [21] Cao B. Master Thesis, Nanjing Technology University, 2007
- [22] Zhao W M, Wang Y, Xue J, Wu K Y. Acta Metall Sin, 2005; 41: 178
- [23] Pourbaix M. Atlas of Electrochemical Equilibria in Aqueous Solutions. New York: Pergamon Press, 1966: 15
- [24] Sasaki T, Kanagawa R, Ohtsuka T, Miura K. Corros Sci, 2003; 45: 847
- [25] Yan Z, Xian A P. Trans Nonferrous Met Soc, 2012; 22: 1398
- [26] Mori M, Miura K, Sasaki T, Ohtsuka T. Corros Sci, 2002; 44: 887
- [27] Chang H, Chen H T, Li M Y, Wang L, Fu Y G. J Electron Mater, 2009; 38: 2170

Note: Figure translations are in progress. See original paper for figures.

Source: ChinaXiv – Machine translation. Verify with original.